Role of reverse shocks for the production of galactic cosmic rays in SNRs

V.N.ZIRAKASHVILI, V.S.PTUSKIN
DOI: 10.7529/ICRC2011/V06/0837
Pushkov Institute of Terrestrial Magnetism, Ionosphere and Radiowave Propagation, 142190, Troitsk, Moscow Region, Russia

Abstract: The production of galactic cosmic rays is investigated using the numerical modeling of the diffusive shock acceleration at forward and reverse shocks in supernova remnants. It is shown that the reverse shocks can be the main source of cosmic ray positrons and heavy nuclei.

Keywords: CR origin, CR acceleration, SNRs

Introduction

The diffusive shock acceleration (DSA) process [10, 2, 3, 7] is considered as the principal mechanism for the production of galactic cosmic rays (CR) in supernova remnants (SNRs). A large theoretical progress in the investigation of this mechanism was achieved during last decades (see e.g. Malkov & Drury [11] for a review).

Two shocks are produced by super-sonically moving supernova ejecta after a supernova explosion. A forward shock propagates in the circumstellar medium while a reverse shock propagates in the gas of ejecta. Some part of thermal particles is injected at the shock fronts into acceleration.

In this paper we investigate the role of the reverse shock in the nonlinear DSA in SNRs. Our model is a natural development of the existing models [4, 9]. The solution of spherically symmetric hydrodynamic equations is combined with the energetic particle transport and acceleration on the forward and reverse shocks of a supernova remnant.

Earlier study has already dealt with the CR spectra produced in SNRs [6, 17, 14]. The input of the reverse shock was not taken into account while the acceleration by both shocks was considered for the modeling of non-thermal emission from the SNR RX J1713.7-3946 [18].

Model of nonlinear DSA

Hydrodynamical equations for the gas density $\rho(r,t)$, gas velocity $u(r,t)$, gas pressure $P_g(r,t)$, and the equation for isotropic part of the CR proton momentum distribution $N(r,t,p)$ in the spherically symmetrical case are given by

$$\frac{\partial \rho}{\partial t} = -\frac{1}{r^2}\frac{\partial}{\partial r} r^2 u \rho \tag{1}$$

$$\frac{\partial u}{\partial t} = -u\frac{\partial u}{\partial r} - \frac{1}{\rho}\left(\frac{\partial P_g}{\partial r} + \frac{\partial P_c}{\partial r}\right) \tag{2}$$

$$\frac{\partial P_g}{\partial t} = -u\frac{\partial P_g}{\partial r} - \frac{\gamma_g P_g}{r^2}\frac{\partial r^2 u}{\partial r} - (\gamma_g - 1)(w-u)\frac{\partial P_c}{\partial r} \tag{3}$$

$$\frac{\partial N}{\partial t} = \frac{1}{r^2}\frac{\partial}{\partial r} r^2 D(p,r,t)\frac{\partial N}{\partial r} - w\frac{\partial N}{\partial r} + \frac{\partial N}{\partial p}\frac{p}{3r^2}\frac{\partial r^2 w}{\partial r}$$
$$+\frac{\eta_f \delta(p-p_f)}{4\pi p_f^2 m}\rho(R_f+0,t)(\dot{R}_f - u(R+0,t))\delta(r-R_f(t))$$
$$+\frac{\eta_b \delta(p-p_b)}{4\pi p_b^2 m}\rho(R_b-0,t)(u(R_b-0,t)-\dot{R}_b)\delta(r-R_b(t)) \tag{4}$$

Here $P_c = 4\pi \int p^2 dpvpN/3$ is the CR pressure, $w(r,t)$ is the advective velocity of CRs, γ_g is the adiabatic index of the gas, and $D(r,t,p)$ is the CR diffusion coefficient. It was assumed that the diffusive streaming of CRs results in the generation of magnetohydrodynamic (MHD) waves. CR particles are scattered by these waves. That is why the CR advective velocity w may differ from the gas velocity u. Damping of these waves results in an additional gas heating. It is described by the last term in Eq. (3). Two last terms in Eq. (4) correspond to the injection of thermal protons with momenta $p = p_f$, $p = p_b$ and mass m at the fronts of the forward and reverse shocks at $r = R_f(t)$ and $r = R_b(t)$ respectively. The shocked interstellar gas and gas of ejecta are separated by a contact discontinuity at $r = R_c$. The dimensionless parameters η_f and η_b determine the injection efficiency. Details of the numerical method can be found elsewhere [18, 20].

The equation for ions is similar to Eq. (4). For ions with the mass $M = Am$ and the mass number A it is convenient

to use the momentum per nucleon p and the normalization of the ion spectra N_i to the nucleon number density. Then the number density of ions n_i is $n_i = 4\pi A^{-1} \int p^2 dp N_i$. The ion pressure $P_i = 4\pi \int p^2 dp v p N_i/3$ is also taken into account in the CR pressure P_c.

We shall neglect the pressure of energetic electrons. The evolution of the electron distribution is described by the equation similar to the equation (4) with additional terms describing synchrotron and IC losses.

The magnetic field plays no dynamical role in the model. We shall assume below that the coordinate dependencies of the magnetic field and the gas density coincide upstream and downstream of the forward shock:

$$B(r) = B_0 \frac{\rho}{\rho_0} \sqrt{\frac{\dot{R}_f^2}{M_A^2 V_A^2} + 1},\ r > R_c. \qquad (5)$$

Here ρ_0 is the gas density, B_0 is the magnetic field strength and $V_A = B_0/\sqrt{4\pi\rho_0}$ is the Alfvén velocity in the circumstellar medium. The parameter M_A determines the value of the amplified magnetic field strength. For low shock velocities $\dot{R}_f < M_A V_A$ the magnetic field is not amplified.

A similar equation was used for magnetic field upstream of the reverse shock at $r < R_b$. The regular field of ejecta was taken to be zero in this region. The magnetic field downstream of the reverse shock is as a rule strongly influenced by the Rayleigh-Taylor instability that occurs in the vicinity of the contact discontinuity and that results in the generation of MHD turbulence in this region. So we assume a homogenous magnetic field in the region $R_b < r < R_c$.

We shall use the following diffusion coefficient

$$D = \eta_B D_B \begin{cases} \left(1 + \frac{M_A^2 V_A^2}{\dot{R}_f^2}\right)^g \exp\left(\frac{r - R_f}{\xi_0 R_f}\right),\ r > R_f, \\ \left(1 + \frac{M_A^2 V_A^2}{\dot{R}_f^2}\right)^g,\ R_c < r < R_f, \\ 1,\ R_b < r < R_c, \exp\left(\frac{R_b - r}{\xi_0 R_b}\right), r < R_b. \end{cases} \qquad (6)$$

Here the parameter $g > 0$ depends on the type of nonlinear wave damping that is essential for low velocity shocks $\dot{R}_f < M_A V_A$ when the magnetic field is not amplified. The parameter ξ_0 describes the increase of the diffusion coefficient at large distances upstream of the shocks. The parameter η_B describes the possible deviations of diffusion coefficient from the Bohm value $D_B = vpc/3qB$ for high-velocity shocks. Since the highest energy particles are scattered by small-scale magnetic fields, their diffusion is faster than the Bohm diffusion [16]. The same is true for smaller energy particles because they can be resonantly scattered only by a fraction of the magnetic spectrum. We shall use the value $\eta_B = 2$ and $\xi_0 = 0.05$ throughout the paper.

We shall use the value of parameter $g = 1.5$. It corresponds to the nonlinear wave damping in the weak turbulence theory. Note that a stronger Kolmogorov-type nonlinear damping used by Ptuskin & Zirakashvili [13] corresponds to $g = 3$.

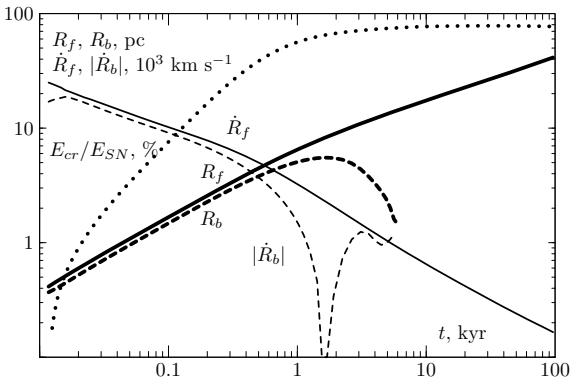

Figure 1: Dependencies on time of the forward shock radius R_f (thick solid line), the reverse shock radius R_b (thick dashed line), the forward shock velocity $\dot{R}_f$ (thin solid line) and the reverse shock velocity $\dot{R}_b$ (thin dashed line). The ratio of CR energy and energy of supernova explosion E_{cr}/E_{SN} (dotted line) is also shown.

Numerical results

Figures (1)-(4) illustrate the numerical results that are obtained for the SNR shock propagating in the medium with the hydrogen number density $n_H = 0.1$ cm^{-3}, the magnetic field strength $B_0 = 5$ μG and the temperature $T = 10^4$ K. The fraction of helium nuclei $x_{He} = n_{He}/n_H = 0.1$ was assumed. We use the ejecta mass $M_{ej} = 1.4 M_\odot$, the energy of explosion $E_{SN} = 1.0 \cdot 10^{51}$ erg and the parameter of ejecta velocity distribution $k = 7$. We used the value of $M_A = 23$. The results of this section are obtained for $w = u$ downstream of the shocks.

The injection efficiency is taken to be independent of time $\eta_b = \eta_f = 0.01$, and the injection momenta are $p_f = 2m(\dot{R}_f - u(R+0,t))$, $p_b = 2m(u(R_b - 0, t) - \dot{R}_b)$. Protons with a mass m are injected at the forward shock while ions with a mass M are injected at the reverse shock. The high injection efficiency results in the significant shock modification already at early stages of SNR expansion while the thermal sub-shock compression ratio is close to 2.5 during the simulation. This is in agreement with the radio-observations of young extragalactic SNRs [8] and with the modeling of collisionless shocks [15].

As for the electron injection we assume a rather high injection energy of electrons $E_{inj} = 100$ MeV. This qualitatively corresponds to models of suprathermal electron injection. Partially ionized ions accelerated at shocks up to relativistic energies may produce multi-MeV electrons in the upstream region in the course of photo-ionization by Galactic optical and infrared radiation [12]. MeV electrons and positrons present in the radioactive supernova ejecta while gamma-rays from ^{56}Co decay in ejecta produce energetic electrons via Compton scattering in the circumstellar medium [19]. These energetic particles may be additionally pre-accelerated via stochastic acceleration in the turbulent upstream regions of the shocks.

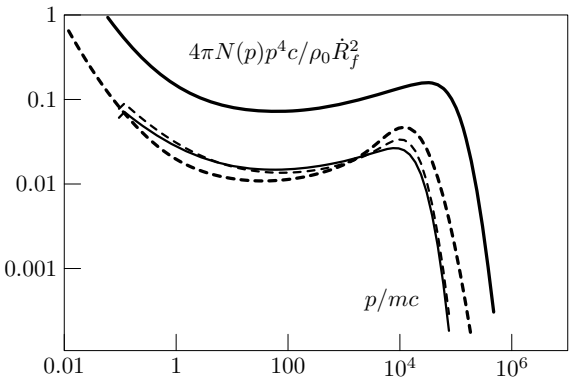

Figure 2: Spectra of accelerated particles at $t = 10^3$ yr. The spectrum of protons at the forward shock (thick solid), the spectrum of ions at the reverse shock (thick dashed), the spectrum of electrons at the forward shock (multiplied on 100, thin solid) and the spectrum of positrons at the reverse shock (multiplied on 100, thin dashed) are shown. The spectrum of ions is the function of momentum per nucleon and is normalized to the nucleon number density.

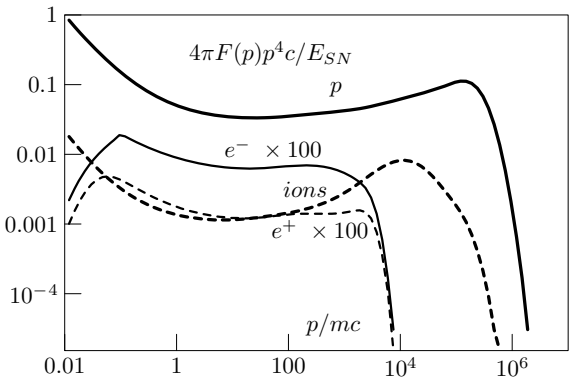

Figure 3: Spectra of particles produced in the supernova remnant during 10^5 yr. The spectrum of protons injected at the forward shock (thick solid line), the spectrum of electrons injected at the forward shock (thin solid line), the spectrum of ions injected at the reverse shock (thick dashed line) and the spectrum of positrons injected at the reverse shock (thin dashed line) are shown. The spectrum of ions is the function of momentum per nucleon and is normalized to the nucleon number density.

Below we assume that electrons are injected at the forward shock with efficiency $\eta_f^- = 10^{-3}\dot{R}_f{}^2/c^2$ while positrons are injected at the reverse shock with efficiency $\eta_b^+ = 10^{-6}$. These numbers are expected for the injection mechanisms mentioned above (see Discussion for details). Since the electrons are considered as the test particles our results may be easily rescaled for any other injection efficiency. The injection rate at the forward shock chosen maintains the electron to proton ratio K_{-p} of the order of $K_{-p} \sim 10^{-3}$ throughout the simulation while the time-independent positron injection at the reverse shock results in the positron to ion ratio K_{+i} increase from $K_{+i} \sim 10^{-4}$ at the very beginning of SNR evolution up to $K_{+i} \sim 10^{-2}$ at the remnant age of several thousand years just before the disappearance of the reverse shock.

The dependencies on time of the shock radii R_f and R_b, the forward and reverse shock velocities $V_f = \dot{R}_f$ and $V_b = \dot{R}_b$, CR energy E_{cr}/E_{SN} are shown in Fig.1. The calculations were performed until the moment of time $t = 10^5$ yr, when the value of the forward shock velocity drops down to $\dot{R}_f = 170$ km s^{-1} and the forward shock radius is $R_f = 41$ pc.

Spectra of accelerated protons and electrons at $t = 10^3$ yr are shown in Fig.2. At this moment of time the maximum energy of protons accelerated in this SNR is close to 100 TeV. The spectra at the reverse shock are harder than the spectra at the forward shock. This is in spite of the same level of the shock modification of the forward and the reverse shocks and is related with the decreasing in time density of the ejecta.

The spectra of particles produced during the whole evolution of the remnant are shown in Fig.3. They are obtained as the sum of the spectra integrated throughout the simulation domain and of the time-integrated diffusive flux at the simulation boundary at $r = 2R_f$. At $t = 10^5$ yr, the maximum energy of currently accelerated particles drops down to 100 GeV because of the nonlinear damping. Higher energy particles have already left the remnant. Note that the stronger Kolmogorov-type damping with $g = 3$ will result even in lower energies of the order of 1 GeV. However we found that the spectra are the same in this case. The faster diffusion assumed upstream of the shocks (see Eq.(6)) results in the lower maximum energy of protons (cf. [6, 17, 14]).

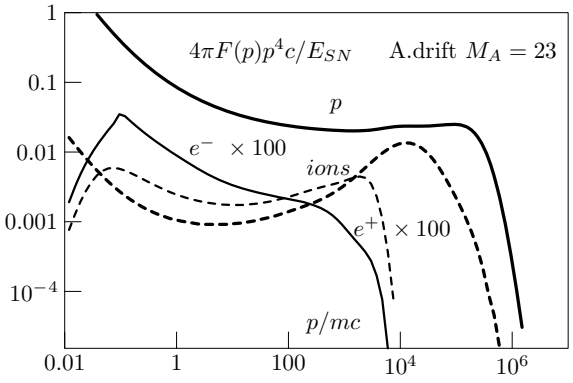

Figure 4: The same as in Fig.3 for the model including the Alfvén drift downstream of the shocks.

Note that the synchrotron losses of run-away electrons and positrons were taken into account in our modeling. That is why the cut-off energy of the leptonic spectra is determined by the magnetic field strength $B_0 = 5\mu$G in the circumstellar medium and by the remnant age $t = 10^5$ yr.

Discussion

Although only about 5% of supernova energy is transferred to the particles accelerated at the reverse shock, they cannot be neglected. First of all the ejecta has an absolutely different composition in comparison with the composition of the interstellar medium where the forward shock propagates. Since the solar abundance corresponds to 1% in the mass of heavy elements while the ejecta can contain up to 50% of heavy elements it is clear that the reverse shock will dominate in the production of heavy CR nuclei.

In addition 70% of supernova energy is transferred to accelerated by the forward shock particles according to our results. It is significantly higher than the estimate of 10-20$\%$ for Galactic CRs. One of possibilities to resolve this contradiction is the assumption that CRs are accelerated only at a small part of the forward shock surface. This can be due to the dependence of the proton and ion injection on the shock obliqueness [5]. This effect is observed in SN 1006 and in the interplanetary medium.

This effect do not influence strongly the ion injection at the reverse shock. It is expected that the random magnetic field is the main component of the field in the expanded ejecta. If so, the relative input of the reverse shock in to the over-all CR spectrum will increase.

Another possibility is related to the Alfvén drift downstream of the forward shock [17]. It results in the steeper spectrum of CRs accelerated at the forward shock. On the other hand the Alfvén drift downstream of the reverse shock can produce even an opposite effect because the CR gradient is positive in this region. As a result the input of the reverse shock will be significant at TeV energies.

The over-all spectrum according to this model is shown in Fig.4. Because of the Alfvén drift the positron spectrum at the reverse shock is significantly harder than the electron spectrum at the forward shock.

We adjust the electron (positron) injection in order to produce a sufficient number of electrons and positrons (see Figs 3,4). This number is enough for the explanation of Galactic CR electrons and positrons. The expected positron injection efficiency from the radioactive decay of ^{44}Ti is estimated as $\eta_b^+ \sim M_{Ti}/(44M_{ej}) \sim 10^{-6}$ [19] for ^{44}Ti mass of the order of $\sim 10^{-4}M_\odot$ as observed in SNRs. So we used a right number in our simulation. As for the electron injection at the forward shock the relative number of energetic electrons from photo-ionization of accelerated single charged He ions is of the order of $\eta_f^- \sim x_{He}\gamma^{-1}\ln^{-1}(p_{max}/mc)\dot{R_f}^2/c^2 \sim 10^{-3}\dot{R}_f^2/c^2$. Here $\gamma \sim I_{He}/\epsilon_{ph} \sim 10$ is the gamma-factor of single-charged He ion photo-ionized by galactic ultraviolet photons with energy $\epsilon_{ph} \sim 10$ eV and $I_{He} = 52$ eV is the ionization potential of helium. Doing so we overestimate the electron injection in young SNRs where the acceleration is fast enough and γ is closer to $\gamma \sim 100$ when the ionization is provided by eV optical photons. However we use this crude estimate that is justified in old SNRs for electron injection in our simulations. This injection mechanism [12] produces one order of magnitude higher number of energetic electrons in comparison with the number $\eta_f^- \sim 10^{-7}R_{f,\mathrm{pc}}^{-2}$ of Compton scattered electrons energized by gamma-photons from ^{56}Co radioactive decay in supernova ejecta [19]. Here $R_{f,\mathrm{pc}}$ is the forward shock radius expressed in parsecs.

Conclusion

Our main conclusions are the following:

1) The reverse shocks in SNRs can give a non-negligible output for the production of CR ions and positrons in comparison with the output of the forward shock.

2) Models of suprathermal electron injection [19, 12] reproduce a required amount of Galactic CR electrons and positrons if the leptons are pre-accelerated up to $E_{inj} \sim 100$ MeV in the upstream regions of supernova shocks.

3) Spectra of particles accelerated at the reverse shock can be harder than the spectra at the forward shock. This is in agreement with the recent Pamela measurements [1] of CR electron to positron ratio and harder observable spectra of CR nuclei.

References

[1] Adriani, O. et al., 2009, Nature 458, 607
[2] Axford, W.I., Leer, E., Skadron, G., 1977, Proc. 15th ICRC, Plovdiv, 90, 937
[3] Bell, A.R., 1978, MNRAS, 182, 147
[4] Berezhko, E.G., Elshin, V.K., Ksenofontov, L.T., 1994, Astropart. Phys. 2, 215
[5] Berezhko, E.G., & Völk, H.J. 2004, A&A 419, L27
[6] Berezhko, E.G. & Völk, H.J. 2007, ApJ, 661, L175
[7] Blandford, R.D., & Ostriker, J.P. 1978, ApJ, 221, L29
[8] Chevalier, R. & Fransson, C., 2006, ApJ 651, 381
[9] Kang, H., Jones, T.W., 2006, Astropart. Phys. 25, 246
[10] Krymsky, G.F. 1977, Sov. Phys.-Doklady, 22, 327
[11] Malkov, M.A., & Drury, L.O'C, 2001, Reports on Progress in Physics, 64, 429
[12] Morlino, G., 2010, arXive:1011.5180
[13] Ptuskin,V.S.,Zirakashvili,V.N.,2005,A&A,429, 755
[14] Ptuskin, V.S., Zirakashvili,V.N., & Seo, E.S., 2010, ApJ, 713, 31
[15] Zirakashvili, V.N. 2007, A&A 466, 1
[16] Zirakashvili, V.N., Ptuskin, V.S., 2008, ApJ 678, 939
[17] Zirakashvili, V.N., Ptuskin, V.S., 2008 Proc. of Intern. Gamma-Ray Symposium, Heidelberg, Germany, 7-11 July 2008, 336
[18] Zirakashvili, V.N., Aharonian, F.A., 2010, ApJ, 708, 965
[19] Zirakashvili, V.N., Aharonian, F.A., 2010, arXive:1011.4775
[20] Zirakashvili, V.N., Ptuskin, V.S., 2011 (in preparation)